Superfast Dipole Inversion (SDI) for real-time Quantitative Susceptibility Mapping (QSM)

Ferdinand Schweser[1], Andreas Deistung[1], Karsten Sommer[1], and Jürgen Rainer Reichenbach[1]
[1]*Medical Physics Group, Dept. of Diagnostic and Interventional Radiology I, Jena University Hospital, Jena, Germany*

INTRODUCTION – Magnetic susceptibility is an intrinsic physical tissue property, which recently became accessible *in vivo* by quantitative susceptibility mapping (QSM) [1]. The practical applicability of QSM, however, is currently hampered by the enormous numerical complexity and computational cost associated with the QSM reconstruction including phase unwrapping, background correction, and field-to-source inversion. Computation times between 30 minutes and several hours for a single dataset currently impede clinical routine application and hinder promising applications, such as QSM-based quantitative fMRI. In this study, we present and analyze a novel QSM framework, *Superfast Dipole Inversion (SDI)*, that not only allows reconstruction of susceptibility maps from raw (wrapped) gradient-echo (GRE) phase data in near real-time, but also enables processing of phase images with open-ended fringe lines [2], which often occur in practice due to improper combination of multi-channel images and which have hitherto hindered QSM. In addition, an approach is presented that allows compensating for intrinsic underestimation of susceptibilities, which has been reported by several authors (e.g. [3]). SDI was evaluated with respect to computation time and reconstruction accuracy based on numerical simulation and volunteer data.

MATERIALS AND METHODS – *Algorithm:* SDI relies on an extension of the background field correction algorithm SHARP [1] and on a combination of SHARP with Thresholded K-Space Division (TKD) [3] for field-to-source inversion. Schweser et al. [4] have recently demonstrated that SHARP may be improved by using the Laplacian kernel instead of a solid sphere kernel during the convolution and deconvolution steps. Schofield and Zhu [5] have shown that the Laplacian $\nabla^2\varphi$ of the phase may be calculated directly from wrapped phase images, φ_w, by using a special non-linear operator L_1: $\nabla^2\varphi = L_1\varphi_w$. The first convolution step in the SHARP algorithm was, thus, replaced by L_1, allowing application of SHARP directly to wrapped phase images. The deconvolution steps of SHARP and TKD were, finally, subsumed in a pre-calculable kernel matrix K. Intrinsic underestimation of susceptibilities by TKD was predicted based on the point-spread function p of the thresholding operation associated with TKD: $p(\vec{r}) = \mathrm{iFT}\left[d(\vec{k})/\tilde{d}(\vec{k})^{-1}\right]$, where $d(\vec{k})$ is the native Fourier dipole response and $\tilde{d}(\vec{k})$ is the thresholded dipole response. The underestimation was compensated for by dividing with $p(0)$.

Data Acquisition and Processing: An *in vivo* reference susceptibility map was acquired from a volunteer (male, 26y) with the COSMOS algorithm [6] according to [1] on a 3 T whole-body MRI scanner (Tim Trio, Siemens Medical Solutions, Erlangen, Germany) using a 12-channel receive head-matrix coil and the ToF-SWI sequence [7]. The following sequence parameters were used: TE_1/TE_2=3.38ms/22ms, TR=30ms, FA=20°, 600µm isotropic voxels, three consecutive scans with -50°, 0°, and 34° tilts of the head around the left-right axis. Multi-channel images were combined using uniform sensitivity reconstruction [8]. To investigate applicability of SDI to phase images with open-ended fringe lines, another volunteer ToF-SWI dataset was acquired (male, 22 years; TE_1/TE_2=12ms/40ms, TR=46 ms, FA=20°, voxel size=470µm×470µm×940µm) and reconstructed neglecting B_1 coil sensitivities.

Evaluation: To assess the computational efficiency of SDI, the algorithm was successively applied to numerical brain model datasets with different matrix sizes ranging from 58x58x38 to 575x575x375 (isotropic voxels; whole brain coverage) and the run time was measured. To investigate reconstruction accuracy, SDI was successively applied with SHARP and TKD regularization parameters t=0…0.05 and d=0…0.7, respectively. Systematic underestimation was assessed by fitting SDI susceptibility values against COSMOS values in several brain regions (ideal reconstruction yields slope s=1.0). Reconstruction artifact level was assessed by the root mean square error (RMSE) relative to the COSMOS map. All data processing was carried out in MATLAB (2010b, The MathWorks, Natick, MA) on a dual-processor workstation with 24 GB RAM.

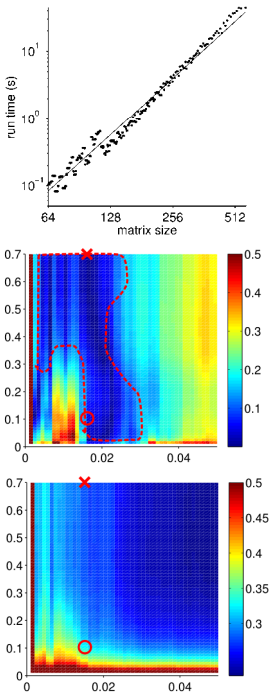

FIGURE 1. Top: Run time of SDI for whole brain coverage (top). Middle and bottom (*d* over *t*): Absolute deviation of fitting slope from one, |s-1|, and RMSE (in ppm).

RESULTS – Run time (Fig. 1-top) was below one second for low-resolution data (<256x256 matrix) and between one and 20 seconds for high-resolution data (>256x256 matrix). Susceptibility estimation was accurate for a wide range of parameters (dotted red outline in Fig. 1-middle), with especially low errors for large values of the TKD-parameter *d* (Fig 1-bottom). Figure 2 illustrates representative transverse slices of the SDI susceptibility maps with d=0.7 (Fig. 2b) and d=0.1 (Fig. 2c). Compared with the COSMOS map (Fig. 2a), the SDI maps were slightly more noisy and suffered from some minor reconstruction artifacts (Fig. 2d). The SDI map with d=0.1 (Fig. 2c) demonstrated streaking artifacts (arrows) and poor cortical contrast. No streaking artifacts were discernable in the SDI map with d=0.7 (see Fig. 2b). Figure 3 demonstrates application of SDI to GRE phase images with open-ended fringe lines. While SDI was able to resolve aliasing in the vicinity of the fringe line (straight arrow in Fig. 3c), an otherwise robust best-path algorithm [9] (applied before SDI) was not (straight arrow in Fig. 3b). Furthermore, SDI was able to resolve phase aliasing in other regions where the best-path algorithm failed due to missing spatial connectivity between different regions, such as in the vicinity of venous vessels, resulting in a more accurate anatomical depiction in the susceptibility map (tailed arrows).

DISCUSSION AND CONCLUSIONS – The proposed QSM framework, SDI, enables fast, accurate, and robust estimation of tissue magnetic susceptibility from a single GRE phase dataset. Due to its numerical simplicity and computational efficiency, SDI not only represents a simple-to-implement tool for researchers hitherto unfamiliar with QSM reconstruction but also enables robust (near) real-time computation of large sets of data. SDI, thus, opens the door for promising advanced applications, such as high-resolution QSM-based fMRI with increased sensitivity [10] or direct implementation of QSM on the MR-scanner hardware for instant reconstruction and displaying of susceptibility maps in a clinical scenario.

REFERENCES – [1] Schweser F et al., 2011. *NeuroImage*. 54:2789-807. [2] Chavez SE et al., 2002. *IEEE Trans Med Imaging*. 21:966-77. [3] Shmueli K et al., 2009. *Magn Reson Med*. 62:1510-22. [4] Schweser F et al. 2011. *ISMRM*. #2667. [5] Schofield MA and Zhu Y. 2003. *Optic Lett*. 28:1194-6. [6] Liu T et al. 2009. *Magn Reson Med*. 61:196-204. [7] Deistung A et al. 2009. *J Magn Reson Imaging*. 29:1478-84. [8] Ros C et al. 2009. *IFMBE Proc*. 22:803-6. [9] Abdul-Rahman HS et al., 2007. *Appl Opt*. 46:6623-35. [10] Petridou N et al., 2009. *Magn Reson Imaging*. 27:1046.

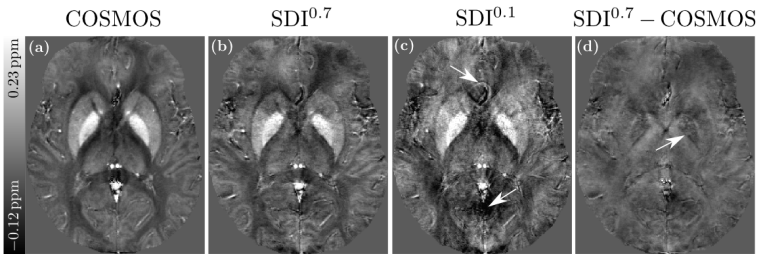

FIGURE 2. Representative slices of QSM reconstructed with COSMOS and SDI. The COSMOS susceptibility map (a) and the susceptibility maps calculated with SDI using thresholding values of 0.7 (b) and 0.1 (c). The difference between COSMOS and SDI with thresholding value 0.7 is shown in (d). Arrows mark reconstruction artifacts. Parameter t was 0.016 in (b) and (c) according to cross and circle in Figure 1.

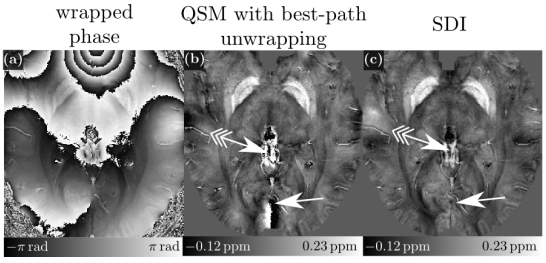

FIGURE 3. Application of SDI to phase data with singularities. The wrapped phase in (a), QSM after applying the 3D best path unwrapping algorithm in (b), the SDI susceptibility map in (c). The straight arrows mark the location of the phase singularity in (a). The tailed arrows mark a region where the best-path algorithm was not able to resolve the phase aliasing.